Conversion-electron extended X-ray absorption fine structure of ion-implanted nanocrystalline evaporated films

1990 J. Phys.: Condens. Matter 2 8113

(http://iopscience.iop.org/0953-8984/2/41/001)

J. Phys.: Condens. Matter **2** (1990) 8113–8122. Printed in the UK

Conversion-electron extended x-ray absorption fine structure of ion-implanted nanocrystalline evaporated films

M Jaouen†, P Bouillaud†, T Girardeau†, P Chartier†, J Mimault† and G Tourillon‡

† Laboratoire de Métallurgie Physique, 40 avenue du Recteur, Pineau, 86022 Poitiers Cédex, France

‡ Laboratoire d'Utilisation du Rayonnement Electromagnétique, Bâtiment 209D, 91405 Orsay Cédex, France

Received 12 September 1989, in final form 1 June 1990

Abstract. Extended x-ray absorption fine-structure (EXAFS) measurements of evaporated and ion-implanted Fe–Co thin films have been obtained by using the conversion-electron detection technique. Experiments were performed on films 700 Å thick in order to get some structural information which may explain their high resistivity value and unusual behaviour after ion–irradiation. Compared with bulk Fe–Co, the electron-beam-evaporated sample yields a damping of the EXAFS signals. We show that this effect is correlated to the nanocrystalline character of the sample so obtained. A quantitative analysis provides an estimation of the grain boundary fraction. Electrical resistivity and EXAFS results suggest that implantations of Fe–Co nanocrystals with heavy ions locally smooth out the insulating effect of the grain boundary but increase the damage produced in the crystalline structure.

1. Introduction

In a previous paper by Rivière *et al* (1990), attention was focused on the electrical resistivity behaviour of electron-beam-deposited Fe–Co thin films. Their static electric resistivity ρ has the surprisingly high value of 118 $\mu\Omega$ cm at 77 K, such a value being more characteristic of those of amorphous materials (for comparison, $\rho = 5.46$ $\mu\Omega$ cm is the value found at 77 K for bulk crystalline Fe–Co alloys of the same composition). Yet, transmission electron microscopy (TEM) patterns recorded on samples formed during the same evaporation run exhibit rings characteristic of the metallic BCC structure. Nevertheless, dark-field images show a material composed of a set of small crystallites whose mean grain size is 8 nm (Rivière *et al* 1990).

When such a thin film is irradiated at 77 K with He^+ or Xe^+ ions, opposite variations in the electrical resistivity ρ are observed: ρ increases for He^+ and, contrary to the expected behaviour, decreases for Xe^+. These effects may be due to the ion self-characteristics (mass and energy), so that different local physical transformations in the matrix result. Therefore, one needs to use a local parameter which is directly related to the microscopic state of the material as a probe.

It is well known that extended x-ray absorption fine structure (EXAFS) is very sensitive to local crystalline disorder or to defects created within the nearest environment of an

0953–8984/90/418113 + 10 $03.50

atomic species. Therefore, this technique is well suited to studying ion irradiation damage through the crystalline matrix and to determine the grain boundary contribution to the measurements. Data have been recorded using conversion-electron extended x-ray absorption fine structure (CEEXAFS) which is well adapted to probing thin films.

The layout of the paper is as follows. First, we recall the basic properties of EXAFS and the specific processes used to output the signal via the CEEXAFS technique. In sections 3 and 4, we describe the sample preparation and the experimental environment. Qualitative and quantitative analyses are performed in section 5 by a careful comparison between the spectra which have been recorded using the same experimental conditions. Finally, in section 6, we discuss the relationship between the EXAFS information and the electrical resistivity behaviour reported by Rivière *et al* (1990).

2. CEEXAFS characteristics

The EXAFS oscillations result in an interference process between the outgoing electron wave and wavelets back-scattered by each neighbour of the central excited atom. X-rays are responsible for atom excitation and EXAFS selects, by tuning the x-ray energy, the type of atom assigned to be the origin of the absorption phenomenon.

The Fe–Co samples investigated by means of the electrical resistivity technique were 700 Å thick (Rivière *et al* 1990). To remain consistent with this depth, the EXAFS experiments were performed on similar sample thicknesses. So, to obtain structural information from such thin films, EXAFS observations were carried out by detecting conversion electrons created by those escaping from the sample in He gas at atmospheric pressure. They are then collected by a positively biased electrode outside the x-ray beam. The more usual apparatus based on fluorescence or transmission detection modes are inadequate because they required sample thicknesses much larger than those probed here.

The EXAFS signals which result from total electron yield measurements have been theoretically described by Lee *et al* (1981). For very thin samples, the product $\mu(E)a$ is so small that it can be assumed proportional to the ratio $I(E)/I_o(E)$. Here $\mu(E)$ and a denote the absorption coefficient at energy E and the sample thickness respectively; $I(E)$ is the total yield current recorded with a DC Keithley nanoammeter and $I_o(E)$ the output signal measured from an ionisation chamber set in the incident beam path.

Since the pioneering work of Koddesh and Hoffman (1984), the CEEXAFS technique has been applied to numerous systems. However, the general shape of $I(E)/I_o(E)$ versus the energy E was never truly consistent with the theoretical absorption coefficient behaviour. Generally, it results in a reduction in EXAFS amplitudes, but fortunately no change in the oscillation phase; extracted coordination numbers must be carefully considered. In fact, when one wishes to extract the EXAFS signal $\chi(E)$ from the data, the most critical step is the normalisation because many different effects contribute to distort the $\mu_0(E)$ background. In particular, the chamber $(I_o(E))$ and the total electron yield device $(I(E))$ do not react identically towards the whole x-ray energy range. Theoretical arguments pointed out by Stöhr *et al* (1974) attribute the generally observed CEEXAFS amplitude reduction to inelastically scattered photoelectrons and these workers suggest an appropriate procedure which can minimise this undesirable effect (normalisation by the K-edge jump). However, this problem remains open since Tourillon *et al* (1987) have shown that the procedure usually used to extract $\chi(E)$ from data in transmission

mode EXAFS leads to correct $\chi(E)$ amplitudes when applied to CEEXAFS data recorded with their electron detector device.

In order to sidestep the question raised by the CEEXAFS amplitude problem discussed above, we have chosen to compare the thin-film CEEXAFS signal with a reference signal recorded in the same experimental x-ray conditions on a bulk sample of the same concentration composed of large crystallites. The protocol used to obtain $\chi(E)$ from the data was the same for all samples so that, if an eventual amplitude reduction exists, it will have the same weight for all spectra owing to the procedure that we used. Thus we believe that differences observed among the spectra presented in the following sections come from different local microscopic structures. In particular, we expect to determine the actual effect of grain boundary interfaces which destroy the interference process and contribute to reducing the oscillation amplitude.

To end this section, as found by Elam *et al* (1987), we have observed that an absorption event created in the material at depth x from the surface generates an electron yield proportional to $\exp(-x/D)$, D being a mean characteristic escape depth for conversion electrons. We assume that the D-values are consistent with the present evaporated sample thicknesses (700 Å). They have been estimated to be approximately 400 Å and 500 Å for the Fe K and the Co K edge, respectively. These values are comparable with those reported by Bouldin *et al* (1987). Details of the method giving these results are not discussed in the present paper and will be developed in a forthcoming paper.

3. Sample preparation

The thin films studied in the present paper were prepared in an ultrahigh-vacuum chamber (Rivière *et al* 1988) by electron beam evaporation from a bulk $Fe_{50}Co_{50}$ alloy. The base pressure during evaporation was about 10^{-9} Torr. Owing to different sputtering rates for Co and Fe atoms, the composition of the resulting films is found to be closer to $Fe_{60}Co_{40}$. The thickness and evaporation rates monitored with a quartz crystal oscillator were chosen to produce samples whose characteristics are those of the alloyed films used in electrical resistivity studies (Rivière *et al* 1990). The substrates, 20 mm long and 10 mm wide, were carefully cleaned in a chemical bath and then in an ultrasonic cleaner. Three films were simultaneously prepared during one evaporation run in order to obtain the same concentration and grain size distribution. One film was analysed without any further treatment and gave the EXAFS signal of the 'evaporated' reference specimen. Ion implantation was performed on the other two films over their whole area. The implantation characteristics are those used for the electrical resistivity studies (Rivière *et al* 1990): He^+ irradiation (2×10^{16} ions cm^{-2}, $E = 15$ keV) and Xe^+ irradiation (1.3×10^{16} ions cm^{-2}, $E = 360$ keV). The incident ion energies were selected in order to generate damage within the whole film thickness. The implantations have been performed at 77 K with very low ion currents in order to prevent beam heating of the target. Subsequently the samples were stored in liquid nitrogen until the EXAFS experiments were carried out. Additional experiments reveal that no apparent evolution occurred in the EXAFS spectra when the samples are kept for a long time at room temperature.

The reference bulk sample was cut from a Fe–Co ingot. Its size was kept identical with those of the previously described substrates. Its surface was mechanically polished with 1200 grit silicon carbide emery paper and then chemically polished in a mixture of

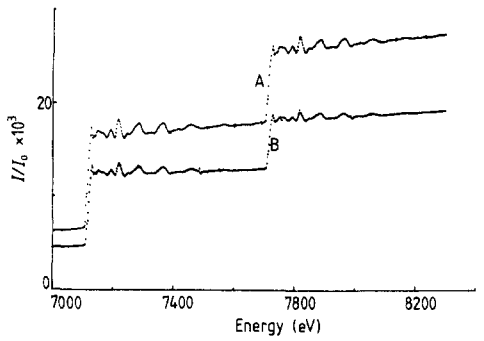

Figure 1. Total electron yield spectra versus energy for Fe–Co samples: spectrum A, 'bulk' sample; spectrum B, thin evaporated film (700 Å).

30 vol.% nitric acid in methanol. Then the sample was homogenised at 700 K in a furnace for 1 h and cooled in ice–water. Crystallites clearly emerge from the surface with an average size of 1 mm.

4. Experimental results

4.1. CEEXAFS experiments

Measurements were performed using the synchrotron radiation from the DCI storage ring (at the Laboratoire pour l'Utilisation du Rayonnement Electromagnétique, Orsay, France) operating with an energy of 1.85 GeV and a current of 230 mA. The electron detector device that we used was described and improved by Tourillon *et al* (1987). In most cases, the evaporation process provides metallic material composed of very small crystallites with random crystallographic orientations. Such a structure has the advantage of eliminating the extra scattering (Bragg) intensity peaks that a large single crystal can produce at some discrete x-ray energy values.

All experiments were performed at room temperature. The simplicity of the technology makes the absorption signal easy to record and allows one to study thin films deposited on glass or quartz substrates without any extra specific preparation.

In order to assure a good signal-to-noise ratio, the electron current is collected over 2 s for each data point, the energy step being 2 eV. The x-ray beam was vertically limited by a slit of 2.5 mm and the samples were tilted at $\theta = 40°$ to offer the best efficiency for the whole beam according to the specimen geometry. Monochromatisation of the incoming beam was achieved with a Si(331) channel-cut monochromator.

4.2. Shapes of CEEXAFS Fe–Co data

The normalised electron yield spectra $I(E)/I_0(E)$ were recorded within the 7000–8500 eV range which includes the Fe K (7111 eV) and the Co K (7709 eV) absorption edges. As seen in figure 1, the experiments provide very similar spectra except in the oscillation amplitudes and in the magnitude ratio of the Fe K to Co K edge jumps. This last parameter is naturally related to the overlayer concentration of the specimen but also results in the film thickness; it is seen to be greater for the bulk (A) sample which is equivalent to a layer of infinite depth. Straightforward calculations based on the escape depths (400 and 500 Å) and the decreasing exponential output electron yield law $dq = q_0 \exp(-x/D)\,dx$ previously mentioned predict a bulk sample ratio $\Delta\mu_{K\,Fe}/\Delta\mu_{K\,Co}$ which

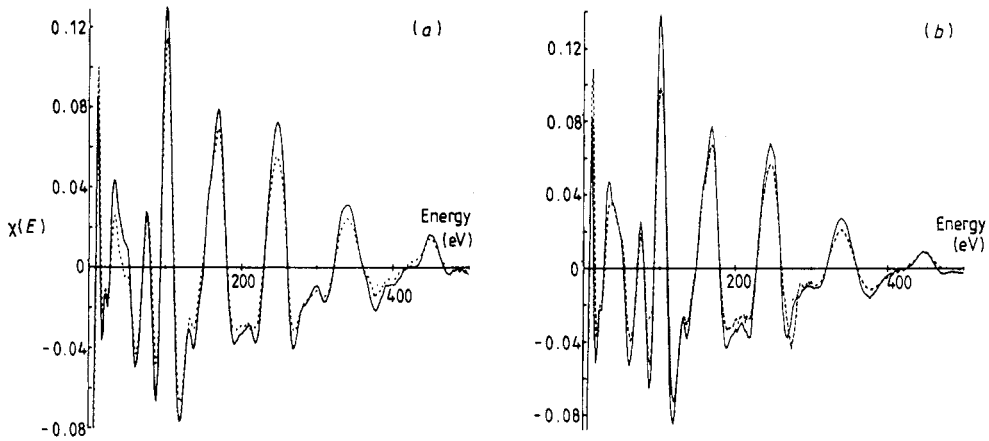

Figure 2. Normalised EXAFS $\chi(E)$ for (*a*) the Fe K edge and (*b*) the Co K edge of Fe–Co samples: ———, 'bulk' samples; – – – –, thin films.

should be 15% smaller than that of the 700 Å thin films. Experimental measurements of the edge jumps also lead to an approximate change of 15% for this ratio.

The background shape versus the x-ray energy increases slightly and monotonically. This behaviour actually differs from the purely theoretical absorption coefficient which, in transmission mode, decreases after each absorption edge. Nevertheless, the shapes of the spectra are always the same for all samples. Since the following quantitative analysis remains comparative, one only needs a consistent method to deduce some local structure changes with confidence and accuracy.

As is well known, the shape and amplitude of the x-ray absorption fine structure result from an interference phenomenon due to the atoms surrounding the excited central atom. At this point, we wish to outline the weak variation in the back-scattering parameters in the present case, the two atomic species here involved being contiguous in the periodic table. Starting with calculated data (McKale *et al* 1986), a rough estimation shows that Fe and Co back-scatterers operate very similarly; their amplitudes differ by less than 5% within the 50–500 eV kinetic energy range while the phase shifts provide a distance shift of about 0.01 Å. So the degree of chemical order does not substantially affect the signal amplitude if the neighbouring shell distances are not sensitive to this parameter. In fact, in the BCC structure, the first- and second-shell back scatterers cannot be separated by the Fourier transform filtering technique. However, any change in neighbour distances must generate a shift in the location of the k-nodes in EXAFS spectra. Obviously, as shown in figure 2, experiments evidenced no such behaviour and we conclude that a variation in the degree of chemical order, if any, does not explain the amplitude degradation of $\chi(E)$ for evaporated samples. The similarity of the two K-edge spectra is also a real indication of the quasi-monatomic behaviour of Fe–Co material for EXAFS studies. So, one must assume that most of the reduction in amplitude observed is undoubtedly induced by significant local disorder in the BCC crystalline structure. The three evaporated specimens (implanted and not implanted) yield the same ratio between the two K edge jumps, and the concentration can be calculated from

$$\Delta(I/I_o)_{Fe}/[\Delta(I/I_o)_{Fe} + \Delta(I/I_o)_{Co}] = 60.1\%.$$

Although this ratio coincides with the expected concentration, the actual value can

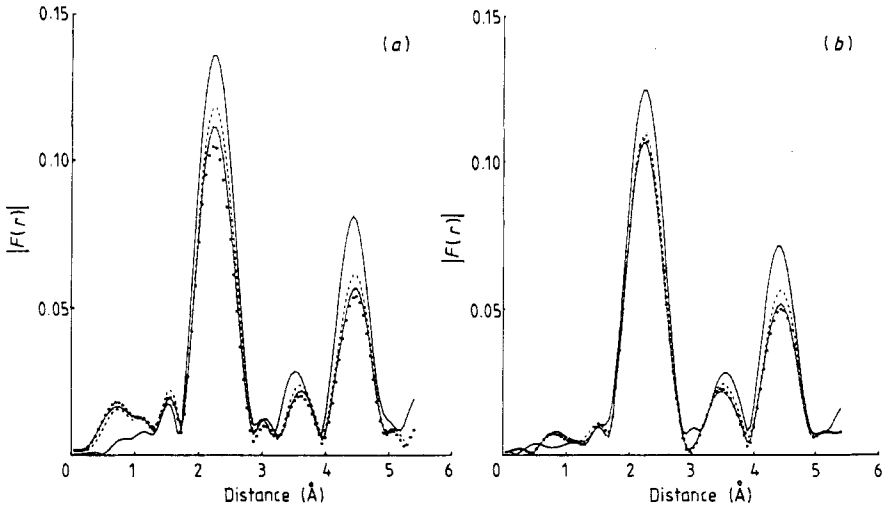

Figure 3. Fourier transform $|F(r)|$ for (*a*) the Fe K edge and (*b*) the Co K edge of Fe–Co samples: ———, 'bulk' samples; – – – –, evaporated thin films; — — —, He^+-implanted thin films; ×, Xe^+-implanted thin films.

be slightly different, for several factors (such as the specific Co K or Fe K absorption step, the Auger energy, the escape depth of each atom species and the ionisation chamber output) must be involved in a quantitative analysis. However, and this is the main result of our work, the quasi-equality of the ratios of the three samples indicates that they all have the same concentration.

5. EXAFS analysis

The procedure used to extract from the data the EXAFS contribution from a single shell (or many nearest shells) has been previously reported (Fontaine *et al* 1979). Figures 3(*a*) and 3(*b*) show the absolute values of Fourier-transformed $k^3\chi(k)$ data recorded for four experimental specimens, for Fe K and Co K edges, respectively. Using the extreme *k*-node location, $k^3\chi(k)$ signals were delimited by the same flat window which was ended by cosines. A simple qualitative comparison between the different Fourier transforms shows an obvious modification of the amplitudes of the peaks; the 'evaporated' signal is significantly reduced with respect to the 'bulk' signal which represents the CEEXAFS reference sample. Ion implantation enhances this phenomenon and the decrease in the additional peaks results from the crystalline damage induced by ion bombardment. Nevertheless, the main effect comes from the evaporation process. The damping is also gradually emphasised according to the distance from the central excited atom; this behaviour is roughly consistent with small crystallite size which involves a noticeable surface-to-volume ratio. The first and third main peaks remain centred for all samples here analysed and for the two K edges. In marked contrast, the second peak exhibits a singular behaviour, shifting towards larger distances for the Fe K edge and in the opposite direction for the Co K edge. This is the only apparent misfit between the two K-edge data. The specific analysis of this phenomenon is not straightforward since the second peak has as its origin both single- and double-back-scattering effects and the

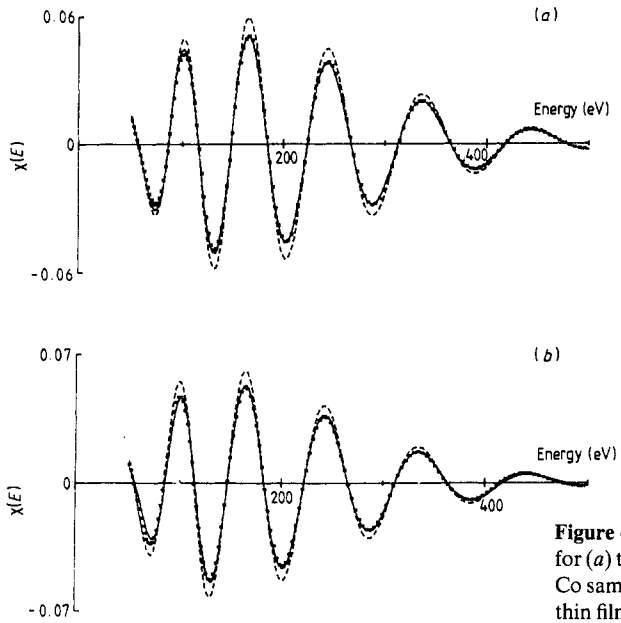

Figure 4. Filtered backtransformed spectra $\chi(E)$ for (*a*) the Fe K edge and (*b*) the Co K edge of Fe–Co samples: – – –, 'bulk' samples; ×, evaporated thin films; ———, 85% of 'bulk' spectrum.

usual EXAFS formulation is unsuitable for a quantitative explanation of these opposite shifts. However, the first peak, which is only due to single back scattering, does not show such variations and we conclude that bond lengths are quasi-unaffected by evaporation or implantation processes. So we suggest that the discrepancies evidenced in the second peak shape originate from the important double-scattering $(r_1 + r_2 + r_1)$ path length contribution, r_1 and r_2 being the nearest- and next-nearest-neighbour distances, respectively. Furthermore, to continue with this double-scattering problem which is strongly connected to the local disorder, it would be more judicious to use a $k\chi(k)$ Fourier transform.

The observed reduction in EXAFS amplitude may arise from several physical origins. First, one could think that significant local disorder exists in the crystalline matrix which acts as an extra Debye–Waller factor. Secondly, one can evoke the crystallite sizes and forms, which modify the resulting amplitudes of the whole sample through the surface-to-volume ratio. Additionally, the nanocrystal grain boundary fraction can contribute a significant amount to the signal; their disorganised or partially organised microscopic structure naturally has a reduction effect on the experimental EXAFS data. Quantitative examination of the amplitude magnitude versus kinetic energy must allow one to discriminate between the different above-mentioned arguments or, at least, to determine the most important. The Fourier back-transformed spectra of the first filtered peak for 'bulk' and 'evaporated film' specimens are shown in figure 4. Clearly, the two EXAFS spectra have a similarity ratio which remains roughly constant within the whole energy range analysed. The two K-edge figures yield the same reduction percentage of 15% for the nanocrystal EXAFS signal with respect to the 'bulk' crystal signal. Such behaviour is inconsistent with the assumption of a simple additive Debye–Waller term (first point above) the weight of which increases gradually with increasing energy. Conversely, the EXAFS amplitude reduction is in full agreement with an artificial reduction in the coordination number. It should be pointed out here that an annealing

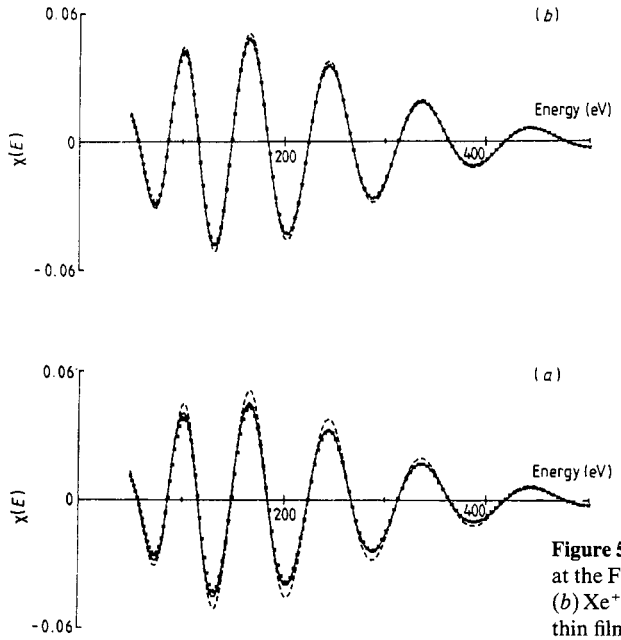

Figure 5. Filtered back-transformed spectra $\chi(E)$ at the Fe K edge (*a*) He^+-implanted thin film and (*b*) Xe^+-implanted thin film: — — —, evaporated thin films; ×, implanted thin films; ———, 88% in (*a*) and 81% in (*b*) of the 'bulk' spectra.

treatment above 450 °C of the thin evaporated film leads to a sample exhibiting the EXAFS behaviour of bulk $Fe_{60}Co_{40}$, e.g. it restores the EXAFS amplitude. To understand the reduction found here, the surface-to-volume ratio has been estimated using the TEM image of a sample evaporated in the same experimental conditions (Rivière *et al* 1990). From TEM images, the size distribution of crystallites exhibits a peak at about 8 nm with a long tail towards higher values. Assuming that all atoms inserted between two spheres whose radii are R and $R - a/2$ are surface atoms (a is the lattice parameter), we have calculated the percentage of atoms constituting the crystallite surfaces. A fraction of the neighbours of these particular atoms have lost their periodic crystalline regularity. An overestimation which corresponds to the extreme case of atoms belonging to the {100} surface plane yields a reduction in the EXAFS amplitudes of about 5%. The previously mentioned asymmetric size dispersion for crystallites slightly decreases the surface-to-volume ratio but does not change it significantly. Thus, we conclude that two thirds of the amplitude reduction found here (e.g. 10% of the bulk) derives from grain boundaries where atoms are spatially disorganised or included in an expanded and distorted lattice. These particular atoms do not contribute constructively to the EXAFS oscillations of a pure BCC structure.

If now we turn to the ion implantation effect, it looks rather discrete for the Co K edge EXAFS spectra but produces different amplitude reductions according to the ion dose at the Fe K edge as is shown in figure 3.

Such a singular behaviour suggests that ion implantation may induce a modification of the concentration inside the crystalline material. Figure 5 again shows a quasi-proportionality between all spectra in the whole energy range and this can be interpreted as a direct indication of the expansion of the non-crystalline volume. It should be pointed out that the EXAFS amplitude reduction is enhanced if irradiation is performed with

Table 1. Evolution of the two parameters required to understand the EXAFS amplitude behaviour.

Sample	Fe-to-Co crystallite concentration	Grain boundary fraction (%)
Evaporated	60 to 40	10
He^+ implanted	59 to 41	12
Xe^+ implanted	57 to 43	19

heavy Xe^+ ions. Table 1 lists the evolution of the two parameters required in order to understand the EXAFS amplitude behaviour with respect to the process involved: evaporation or ion irradiation. Calculations have been performed keeping an unchanged crystallite average size (surface-to-volume ratio) and an atomic Fe-to-Co concentration of 60 to 40 for the 'evaporated' specimen.

6. Discussion

Compared with the EXAFS spectrum recorded for a Fe–Co sample cut from an ingot cast in a classic way, thin evaporated films provide reduced but quasi-proportional signals. These results are similar to those obtained by Haubold *et al* (1989) with Cu nanocrystalline materials produced by an inert-gas condensation technique. The chemical local order is not responsible for the amplitude decrease. This effect unambiguously corresponds to a significant grain boundary volume the atomic structure of which is partially or completely random. The absolute values listed in table 1 are greater than the error bars, and the comparison between successive spectra clearly shows that the same degradation phenomenon is involved in evaporated film as well as in ion-irradiated films. A macroscopic model which would include idealised cubic crystallites of 8 nm well delimited by faceted boundaries shows that a loss of 10% of the BCC structure is equivalent to 1.5 additional atomic spacings between two contiguous cubes. The high resistivity value found for such a structure suggests that, between crystallites, a rather continuous medium constituted of randomly distributed atoms exists. These separations are rarely interrupted by crystalline connections so that a low electrical conduction for the whole film results. One observes variations in ρ versus ion dose of such a nature that, on the one hand, it increases initially and then decreases for Xe^+ while, on the other hand, it always increases for He^+ (Rivière *et al* 1990, figures 5 and 6). Among the agglutinated crystallites embedded in a disorganised medium, as defined above, an irradiation process is more or less efficient according to the kinetic energy of incoming ions, and EXAFS results seem consistent with the well known fact that the damage created is more important for 360 keV Xe^+ ions than for 15 keV H^+ ions (table 1). However, the electrical resistivity records do not follow such a simple law. A coherent interpretation of both EXAFS and electrical resistivity data must include the individual collision cascade volume and the energy dissipation density as parameters, these being substantially greater for a Xe^+ impinging ion than for a He^+ one. In this latter case, one can effectively consider that the damage essentially consists of random atom displacements through the whole solid, resulting in a much distorted crystallite surface and more local defects in the crystalline medium. The EXAFS change is too small to yield more precise information

but, when described using the 'thermal spike' concept (Diaz de la Rubia *et al* 1989), Xe^+ incident ions give rise to a localised region with a temperature enhancement large enough to remove momentarily the crystalline structure. The subsequent ultrafast freezing is generally characterised by increasing structural disorder, the remaining non-crystalline volume depending on complex processes occurring during the solidification kinetics. Such an effect generates an amplitude degradation of the EXAFS signal which is very sensitive to the topological disorder. Nevertheless, when melt zones are created extending across the grain boundaries, the recrystallisation volume could grow between two adjacent grains and it can provide a new better electrical connection within the specimen. The electrical resistivity parameter is undoubtedly very sensitive to these new high-conduction paths.

The crystalline concentration change is an original and new result which seems particularly unambiguous after Xe^+ ion implantation. One can suggest that recrystallisation results in a concentration much closer to that of an equiatomic alloy and rejects outside the cascade volume the unwanted Fe atoms.

7. Conclusion

In this paper, we have studied thin films of $Fe_{60}Co_{40}$ alloy produced by electron beam evaporation under ultrahigh vacuum. Using EXAFS in the conversion-electron mode, we have shown that such as-evaporated films exhibit the structure of nanocrystalline materials. As suggested by Birringer (1989, and references therein) the nanocrystal consists of two components: a crystalline component formed of well crystallised small grains (8 nm) and an interfacial component or grain boundary with a random atomic arrangement. By comparison with the CEEXAFS signal provided by a bulk sample, we have quantised the fraction of randomly distributed atoms in as-evaporated $Fe_{60}Co_{40}$ thin films. The topological order of the crystallised grains was found to be that of bulk $Fe_{60}Co_{40}$. The effects of He^+ or Xe^+ ion implantation have been investigated in the same way. In order to understand the EXAFS and electrical resistivity behaviours of ion-irradiated films, a conduction model based on a percolation approach is propounded (Rivière *et al* 1990). In particular, both EXAFS and electrical resistivity results suggest that thermal spikes generated by Xe^+ ion implantation create structural disorder through the crystalline matrix, but they also partly remove the strong insulating character of the primitive grain boundary.

References

Bouldin C E, Forman R A and Bell M I 1987 *Phys. Rev.* B **35** 1429
Birringer R 1989 *Mater. Sci. Eng.* A **117** 33–43
Diaz de la Rubia T, Averback R S and Hsied H 1989 *J. Mater. Rev.* **4** 579
Elam W T, Kirkland J P, Neiser R A and Wolf P D 1988 *Phys. Rev.* B **38** 579
Fontaine A, Lagarde P, Raoux D and Spanjaard D 1979 *Phil. Mag.* B **40** 17
Haubold T, Birringer R, Lengeler B and Gleiter H 1989 *Phys. Lett.* **135** 461
Koddesh M E and Hoffman R W 1984 *Phys. Rev.* B **29** 491
Lee P A, Citrin P H, Eisenberger P and Kincaid B M 1981 *Rev. Mod. Phys.* B **5** 769
McKale A G, Knapp G S and Chan S K 1986 *Phys. Rev.* B **33** 841
Rivière J P, Bouillaud P, Dinhut J F, Delafond J 1990 *Radiat. Eff. Defects Solids* **114** 145
Rivière J P, Guesdon Ph, Delafond J and Denanot M F 1988 *J. Less-Common Met.* **145** 477–86
Stohr J, Noguera C and Kendelewicz T 1974 *Phys. Rev.* B **30** 5541
Tourillon G, Dartyge E, Fontaine A, Lemonnier M and Bartol F 1987 *Phys. Lett.* **121A** 251